Supplement of Atmos. Chem. Phys., 25, 15765–15783, 2025 https://doi.org/10.5194/acp-25-15765-2025-supplement © Author(s) 2025. CC BY 4.0 License.





Supplement of

Role of aerosol-cloud-radiation interactions in modulating summertime quasi-biweekly rainfall intensity over South China

Hongli Chen et al.

Correspondence to: Pang-Chi Hsu (pangchi@nuist.edu.cn)

The copyright of individual parts of the supplement might differ from the article licence.

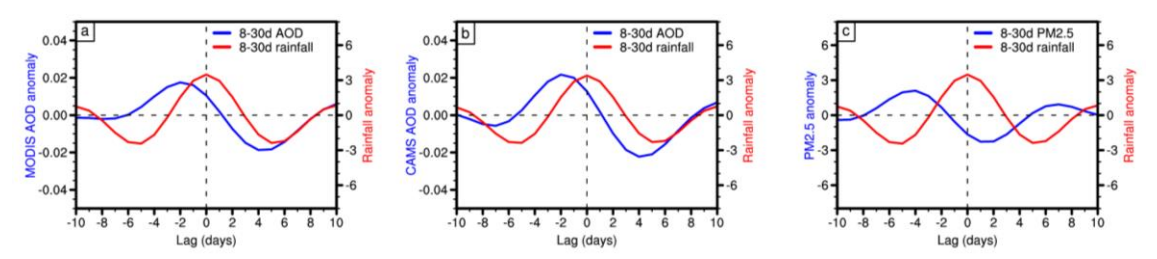


Figure S1. (a) Evolution of 8–30-day precipitation (red curve, mm d⁻¹), MODIS AOD (blue curve, unitless) associated with quasi-biweekly precipitation events, defined as periods with positive 8–30-day rainfall anomalies over South China. Day 0 denotes the peak of rainfall events, while negative and positive values on the x-axis indicate days before and after the peak, respectively. (b) and (c) are similar to (a), but represent the composite results of 8–30-day AOD based on Copernicus Atmosphere Monitoring Service (CAMS) data (Inness et al., 2019) and 8–30-day PM_{2.5} (ChinaHighPM_{2.5}; Wei et al., 2020, 2021; μ g m⁻³), respectively.

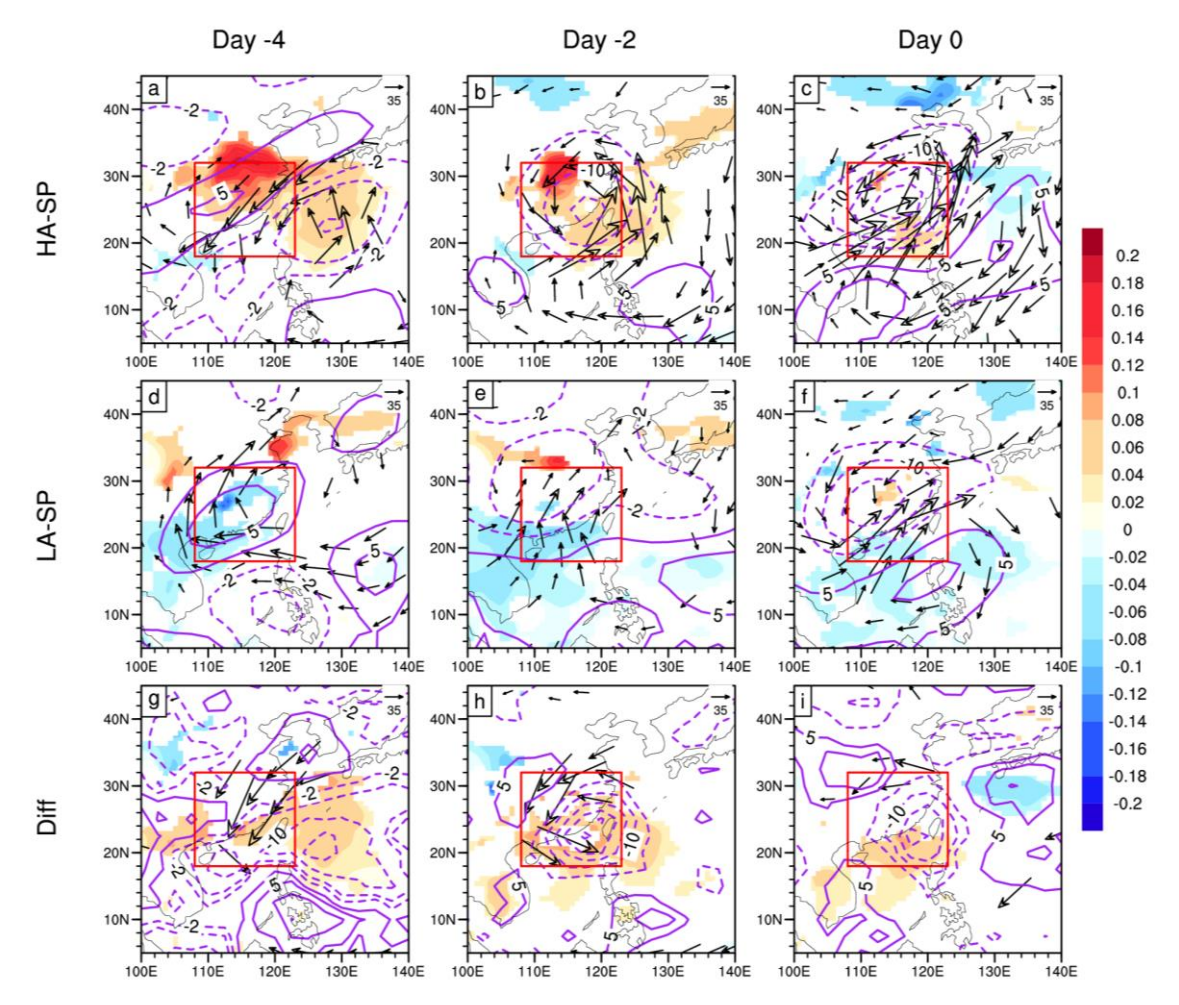


Figure S2. (a)–(c) Composite evolution of 8–30-day outgoing longwave radiation (OLR; purple contours, W m⁻²), AOD (shading, unitless), and column-integrated moisture flux (vectors, kg m⁻¹ s⁻¹) at 4, 2, and 0 days before the occurrence of High AOD–Strong Precipitation (HA–SP) events, respectively. These results are based on NOAA OLR data, ERA5 meteorological data, and CAMS AOD data. (d)–(f) and (g)–(i) Similar to (a)–(c), but for the composite results of Low AOD–Strong Precipitation (LA–SP) and the differences between HA–SP and LA–SP events, respectively. Only AOD and moisture flux anomalies with statistically significant changes at the 90% confidence level are shown. The red box outlines the study domain of South China.

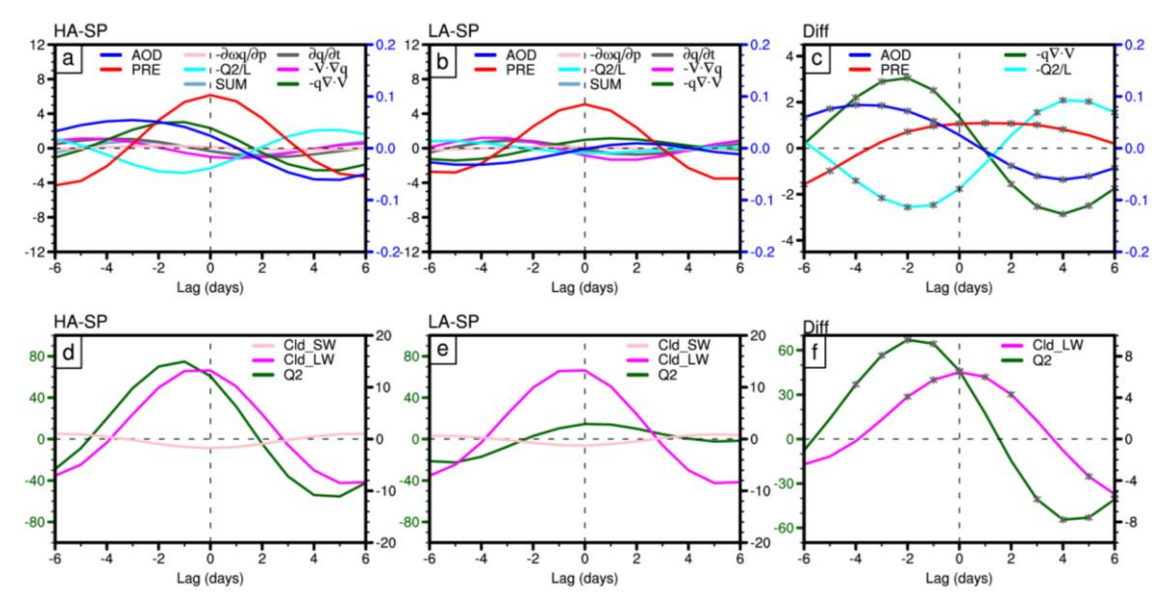


Figure S3. (a) As in Fig. S1a, but for the composite evolution of 8–30-day (a) precipitation (red curve; left *y*-axis, mm d⁻¹), CAMS AOD (blue curve; right *y*-axis in blue, unitless), and individual moisture budget terms based on 0.25°-resolution ERA5 data (various colored curves representing each budget term in Eq. (1); left *y*-axis, mm d⁻¹) associated with HA–SP events. (d) As in (a), except that (d) shows 8–30-day column-integrated latent heat heating (Q_2 ; green curve; left y-axis in green, W m⁻²), 8–30-day longwave and shortwave cloud radiative effects (Cld_LW, magenta curve; Cld_SW, pink curve) calculated from Eq. (2) (right y-axis, W m⁻²). (b, e) and (c, f) are similar to (a, d), but represent the composite results for LA–SP and the differences between HA–SP and LA–SP events, respectively. In panels (c) and (f), only terms with statistically significant differences at the 90% confidence level are shown, with significant periods marked by gray asterisks.

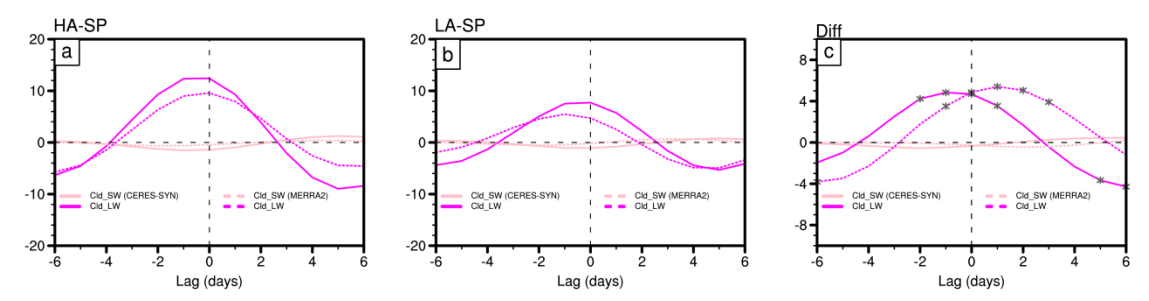


Figure S4. (a) As in Fig. S1a, but for the composite evolution of 8–30-day longwave and shortwave cloud radiative effects (Cld_LW, magenta curve; Cld_SW, pink curve) calculated from Eq. (2) (W m⁻²) derived from CERES-SYN (solid curves) and MERRA-2 (dashed curves), associated with HA–SP events. (b) and (c) are similar to (a), but represent the composite results for LA–SP events and the differences between HA–SP and LA–SP events, respectively. In panel (c), the periods when their differences with statistically significant differences at the 90% confidence level are marked by gray asterisks.

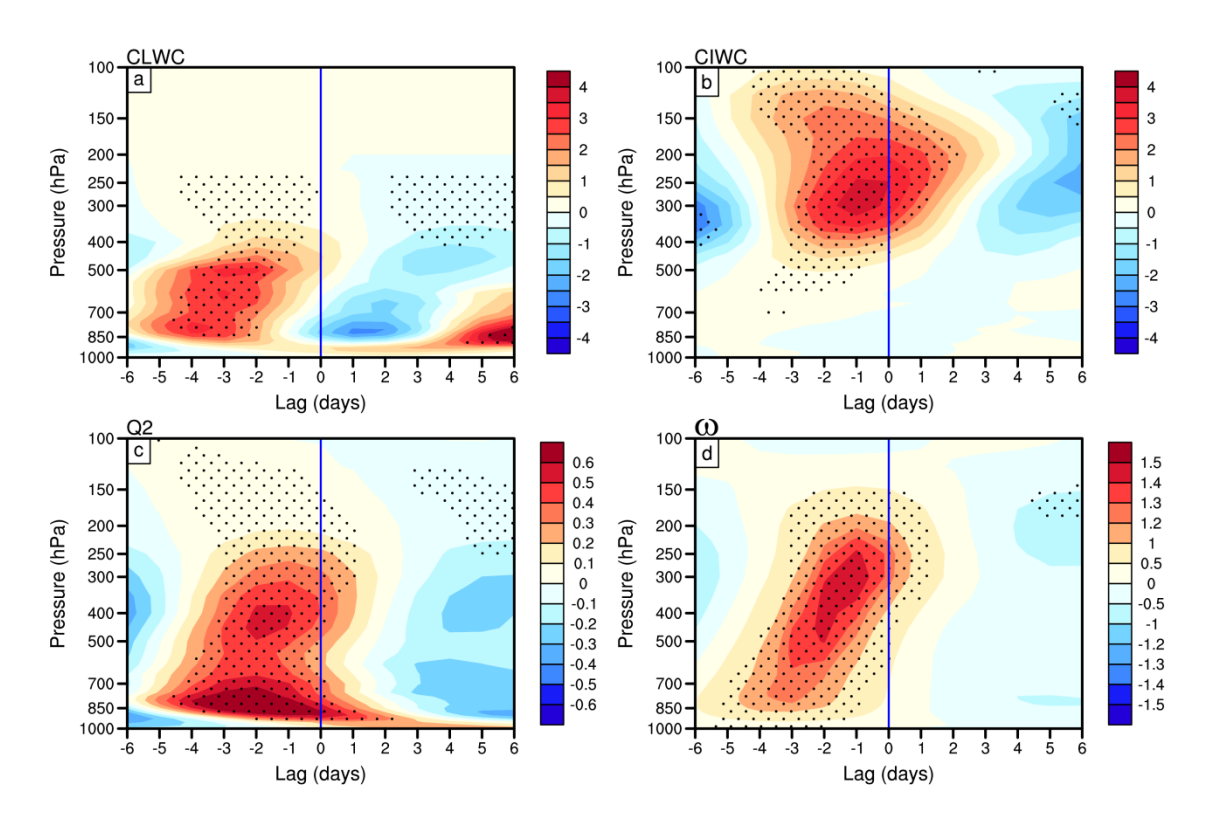


Figure S5. Height–time evolution of 8–30-day anomalies in (a) liquid cloud water content (CLWC; $10^{-6} \, \mathrm{kg \, kg^{-1}}$), (b) ice cloud water content (CIWC; $10^{-6} \, \mathrm{kg \, kg^{-1}}$), (c) latent heat heating (K d⁻¹), and (d) vertical velocity anomalies ($-10^{-2} \, \mathrm{Pa \, s^{-1}}$) between the HA–SP and LA–SP events, based on the ERA5 data. Stippling denotes differences statistically significant at the 90% confidence level. Vertical blue lines denote the peak timing of heavy rainfall event (Day 0).

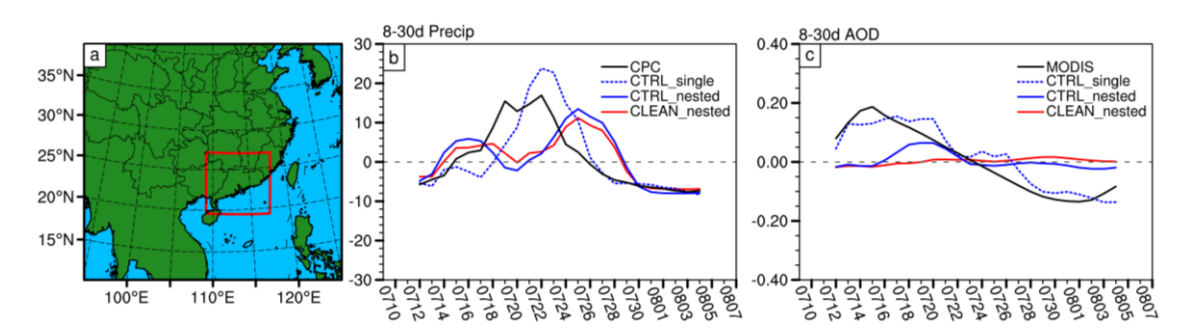


Figure S6. (a) WRF-Chem nested model domains with horizontal resolutions of 20 km (domain 1) and 4 km (domain 2). (b) Evolution of precipitation anomalies (mm d⁻¹) and (c) AOD anomalies (unitless) averaged over the Pearl River Delta (21°–24°N, 111°–116°E). Black curves denote observations (CPC rainfall and MODIS AOD), while blue and red solid curves represent CTRL and CLEAN experiments of the nested-domain simulation, respectively. The CTRL experiment of the single-domain simulation is also shown (blue dashed curves). All experiments are initialized on 9 July 2015.

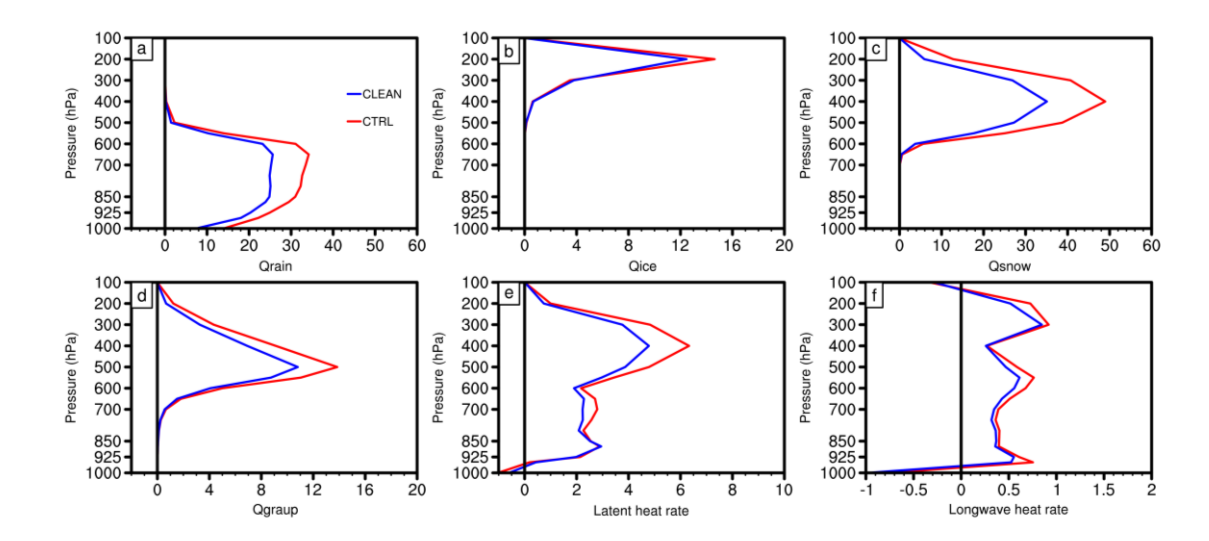


Figure S7. Vertical profiles of (a)–(d) hydrometeor mixing ratio anomalies (10^{-6} kg kg⁻¹) averaged over the key region for the CTRL and CLEAN experiments during 23–26 July 2015 in the nested simulations: (a) raindrop anomalies, (b) cloud ice anomalies, (c) snow anomalies, and (d) graupel anomalies. (e)–(f) As in (a), but for the vertical profiles of (e) latent heat rate anomalies (K d⁻¹), and (f) longwave heat rate anomalies (K d⁻¹).

References

- Inness, A., Ades, M., Agustí-Panareda, A., Barré, J., Benedictow, A., Blechschmidt, A. M., Dominguez, J. J., Engelen, R., Eskes, H., Flemming, J., Huijnen, V., Jones, L., Kipling, Z., Massart, S., Parrington, M., Peuch, V. H., Razinger, M., Remy, S., Schulz, M., and Suttie, M.: The CAMS reanalysis of atmospheric composition, Atmos. Chem. Phys., 19, 3515-3556, https://doi.org/10.5194/acp-19-3515-2019, 2019.
- Wei, J., Li, Z., Cribb, M., Huang, W., Xue, W., Sun, L., Guo, J., Peng, Y., Li, J., Lyapustin, A., Liu, L., Wu, H., and Song, Y.: Improved 1 km resolution PM2.5 estimates across China using enhanced space—time extremely randomized trees, Atmos. Chem. Phys., 20, 3273-3289, https://doi.org/10.5194/acp-20-3273-2020, 2020.
- Wei, J., Li, Z., Lyapustin, A., Sun, L., Peng, Y., Xue, W., Su, T., and Cribb, M.: Reconstructing 1-km-resolution high-quality PM2.5 data records from 2000 to 2018 in China: spatiotemporal variations and policy implications, Remote Sens. Environ, 252, 112136, https://doi.org/10.1016/j.rse.2020.112136, 2021.